

Tight Mutual Information Estimation With Contrastive Fenchel-Legendre Optimization

Qing Guo², Junya Chen¹, Dong Wang¹, Yuewei Yang¹,
Xinwei Deng², Lawrence Carin^{1,3}, Fan Li¹, Chenyang Tao^{1,†}
¹Duke University ²Virginia Tech ³KAUST

Abstract

Successful applications of InfoNCE and its variants have popularized the use of contrastive variational mutual information (MI) estimators in machine learning. While featuring superior stability, these estimators crucially depend on costly large-batch training, and they sacrifice bound tightness for variance reduction. To overcome these limitations, we revisit the mathematics of popular variational MI bounds from the lens of unnormalized statistical modeling and convex optimization. Our investigation not only yields a new unified theoretical framework encompassing popular variational MI bounds but also leads to a novel, simple, and powerful contrastive MI estimator named as FLO. Theoretically, we show that the FLO estimator is tight, and it provably converges under stochastic gradient descent. Empirically, our FLO estimator overcomes the limitations of its predecessors and learns more efficiently. The utility of FLO is verified using an extensive set of benchmarks, which also reveals the trade-offs in practical MI estimation.

1 Introduction

Assessing the dependency between pairs of variables is integral to many scientific and engineering endeavors [1, 2]. *Mutual information* (MI) has been established as a popular metric to quantify generic associations [3], and its empirical estimators have been widely used in applications such as independent component analysis [4], fair learning [5], neuroscience [6], Bayesian optimization [7], among others. Notably, the recent advances in deep *self-supervised learning* (SSL) heavily rely on the success of nonparametric MI optimization [8–12]. In this study, we focus on the discussion in the likelihood-free variational approximation of MI using only paired samples.

Given its importance, MI estimation has been extensively studied over the years [13, 14, 3, 15–17]. While most classical estimators work reasonably well for low-dimensional cases, they scale poorly to big, complex datasets: naïve density-based estimator(s) and k -nearest neighbor estimators [18–20] struggle with high-dimensional inputs, while kernel estimators are slow, memory demanding and sensitive to hyperparameters [21, 22]. Moreover, these estimators are usually either non-differentiable or need to hold all data in memory. Consequently, they are not well suited for emerging applications where the data representation needs to be differentiably optimized based on small-batch estimation of MI [23]. Alternatively, one can approach MI estimation through use of an estimated likelihood ratio [24, 23], but the associated numerical instability has raised concerns [25].

To scale MI estimation to the ever-growing size and complexity of modern datasets, also further to accommodate the need for representation optimization [26], variational objectives have become widely utilized in recent years [9]. Instead of the direct estimation of densities, their ratios or the corresponding gradients [27], these approaches appeal to various variational inequalities to construct tractable lower or upper bounds of the mutual information [28], facilitated by the use of auxiliary

critic functions¹. This practice turns the estimation of MI into an optimization problem. Prominent examples in this category include the *Barber-Agakov* (BA) estimator [29], the *Donsker-Varadhan* (DV) estimator [30], and the *Nguyen-Wainwright-Jordan* (NWJ) estimator [31]. Notably, these variational estimators closely connect to the variational objectives for likelihood inference [32].

Despite reporting significant success, a major difficulty with these variational estimators has also been recognized: their estimation variance grows exponentially to the ground-truth MI [33]. This is especially harmful to applications involving deep neural nets, as it largely destabilizes training [34]. An effective fix to this variance issue is to leverage multi-sample contrastive estimators, pioneered by the work of *InfoNCE* [9]. However, the massive reduction in the variance comes at a price: the performance of *InfoNCE* estimator is upper bounded by $\log K$, where K is the number of *negative* samples used [28]. For a large MI, this K needs to be sufficiently large to allow for an adequate estimate, consequently constructing a significant burden on computation and memory. While variants of *InfoNCE* have been motivated to achieve more controllable bias and variance tradeoffs [28, 34], little research has been conducted on the cost-benefit aspect of contrastive learning.

Notably, a critical insight enabled by *InfoNCE* is that mutual information closely connects to contrastive learning [35, 9]. Paralleled by the empirical successes of instance discrimination-based self-supervision [36, 37, 11, 10] and multi-view supervision [38, 39], *InfoNCE* offers an *InfoMax* explanation to why the ability to discriminate naturally paired *positive* instances from the randomly paired *negative* instances leads to universal performance gains in these applications [40, 41, 28]. Despite these encouraging developments, the big picture of MI optimization and contrastive learning is not yet complete: (i) there is an ongoing debate about to what extent MI optimization helps to learn [42]; (ii) how does the contrastive view reconcile with those non-contrastive MI estimators; and crucially, (iii) are the tradeoffs made by *InfoNCE* absolutely necessary?

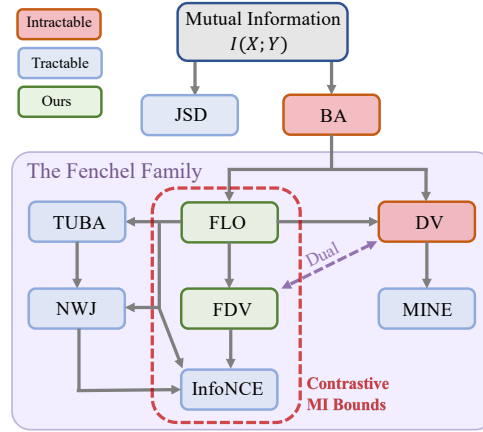


Figure 1: Schematic of variational lower bounds of mutual information. FLO provides a novel unified framework to analyze contrastive MI bounds.

In this work, we seek to bridge the above gaps in the current literature by approaching the MI estimation from the novel perspective of energy modeling. While this subject has already been extensively studied using information-theoretic and variational inequalities, we embrace a new view from the lens of unnormalized statistical modeling. In particular, we highlight the following interesting discoveries: (i) unification of popular variational MI bounds under unnormalized statistical modeling; (ii) derivation of a simple but powerful new contrastive variational bound called FLO; (iii) justification on the theoretical properties of the FLO bound such as tightness and convergence; and (iv) demonstration of strong empirical evidence that the performance of this new FLO bound supersedes its predecessors in practice. Further, to lend a solid footing for representation optimization literature, we also contribute in-depth discussion to bridge the gaps between contrastive learning and MI estimation, along with principled practical guidelines informed by theoretical insights.

2 Fenchel-Legendre Optimization for Mutual Information Estimation

2.1 Preliminaries

This section briefly reviews the mathematical backgrounds needed for our subsequent developments.

Unnormalized statistical modeling defines a rich class of models of general interest. Specifically, we are interested in the problem for which the system is characterized by an energy function $\tilde{p}_\theta(x) : \mathcal{X} \rightarrow \mathbb{R} : \exp(-\psi_\theta(x))$, where θ is the system parameters and $\psi_\theta(x)$ is known as the *potential function*. The goal is to find a solution that is defined by a normalized version of $\tilde{p}_\theta(x)$, i.e.,

$$\min_{\theta} \{\mathcal{L}(p_\theta)\}, \text{ subject to } p_\theta(x) = \frac{\tilde{p}_\theta(x)}{Z(\theta)}, \quad Z(\theta) \triangleq \int \tilde{p}_\theta(x') d\mu(x'), \quad (1)$$

¹When estimates are sharp, these critic functions usually recover some transformation of the likelihood ratio.

where $\mathcal{L}(\cdot)$ is the loss function, μ is the base measure on \mathcal{X} and $Z(\theta)$ is called the partition function. Problems in the above form arise naturally in maximal likelihood estimation [43], Bayesian analysis [44] and statistical physics [45]. A major difficulty with unnormalized statistical modeling is that the partition function $Z(\theta)$ is generally intractable for complex energy functions², and in many applications $Z(\theta)$ is further composed by $\log(Z_\theta)$, whose concavity implies any finite sample estimate Monte-Carlo of $Z(\theta)$ will render the \mathcal{L} biased. Bypassing the difficulties caused by the intractable partition function is central to unnormalized statistical modeling.

Mutual information and unnormalized statistical models We first establish the connection between MI estimation and unnormalized statistical modeling. As a generic score assessing the dependency between two random variables (X, Y) , *mutual information* is formally defined as the *Kullback-Leibler divergence* (KL) between the joint distribution $p(x, y)$ and product of the respective marginals $p(x)p(y)$ [2], i.e., $I(X; Y) \triangleq \mathbb{E}_{p(x, y)} \left[\log \frac{p(x, y)}{p(x)p(y)} \right]$. The integrand $\log \frac{p(x, y)}{p(x)p(y)}$ is often known as the *point-wise mutual information* (PMI) in the literature. Mutual information has a few appealing properties: (i) it is invariant wrt invertible transformations of x and y , and (ii) it has the intuitive interpretation of reduced uncertainty of one variable given another variable³.

To connect MI to unnormalized statistical modeling, we consider the classical *Barber-Agakov* (BA) estimator of MI [46]. To lower bound MI, BA introduces a variational approximation $q(y|x)$ for the posterior $p(y|x)$, and by rearranging the terms we obtain the following inequality

$$\begin{aligned} I(X; Y) &= \mathbb{E}_{p(x, y)} \left[\log \frac{p(y|x)}{p(y)} \right] = \mathbb{E}_{p(x, y)} \left[\log \frac{q(y|x)}{p(y)} \right] + \mathbb{E}_{p(x)} [\text{KL}(p(y|x) \parallel q(y|x))] \quad (2) \\ &\geq \mathbb{E}_{p(x, y)} \left[\log \frac{q(y|x)}{p(y)} \right] \triangleq I_{\text{BA}}(X; Y|q). \end{aligned} \quad (3)$$

Here we have used $I_{\text{BA}}(X; Y|q)$ to highlight the dependence on $q(y|x)$, and this bound is sharp when $q(y|x) = p(y|x)$. Note the naïve BA bound is not useful for sample-based MI estimation, as we do not know the ground-truth marginal density $p(y)$. However, this nuisance can be bypassed by cleverly setting $q_\theta(y|x) = \frac{p(y)}{Z_\theta(x)} e^{g_\theta(x, y)}$, where we call $e^{g_\theta(x, y)}$ the *tilting function* and recognize $Z_\theta(x) = \mathbb{E}_{p(y)} [e^{g_\theta(x, y)}]$ as the *partition function*. Substituting this $q_\theta(y|x)$ into (30) gives the following *unnormalized BA* bound (UBA) that pertains to unnormalized statistical modeling [28]

$$I_{\text{UBA}}(X; Y|g_\theta) \triangleq \mathbb{E}_{p(x, y)} [g_\theta(x, y)] - \mathbb{E}_{p(x)} [\log Z_\theta(x)] = \mathbb{E}_{p(x)} \left[\mathbb{E}_{p(y|x)} \left[\log \frac{\exp(g_\theta(x, y))}{Z_\theta(x)} \right] \right]. \quad (4)$$

This UBA bound is again intractable, but now because of $Z_\theta(x)$ instead of $p(y)$, which is the point we seek to address in this paper. For its connections to other popular MI bounds listed in Table 1, further details are provided in the Appendix.

Noise contrastive estimation and InfoNCE InfoNCE is a multi-sample mutual information estimator proposed in [9] built on the idea of *noise contrastive estimation* (NCE) [35]. With a carefully crafted noise distribution, NCE learns statistical properties of a target distribution by comparing the *positive* samples from the target distribution to the “*negative*” samples from the noise distribution. As such, this technique is also associated with the name *negative sampling* in some contexts [36, 47]. The InfoNCE estimator implements this contrastive idea as follows⁴

$$I_{\text{InfoNCE}}^K(X; Y|f) \triangleq \mathbb{E}_{p^K(x, y)} \left[\log \frac{f(x_1, y_1)}{\frac{1}{K} \sum_{k'} f(x_1, y_{k'})} \right], \quad I_{\text{InfoNCE}}^K(X; Y) \triangleq \max_{f \in \mathcal{F}} \{ I_{\text{InfoNCE}}^K(X; Y|f) \}, \quad (5)$$

where we have used $p^K(x, y)$ to denote K independent draws from the joint density $p(x, y)$, and $\{(x_k, y_k)\}_{k=1}^K$ for each pair of samples. Here the positive and negative samples are respectively drawn from the joint $p(x, y)$ and product of marginals $p(x)p(y)$. Intuitively, InfoNCE tries to accurately classify the positive samples when they are mixed with negative samples using the CrossEntropy loss. The Proposition below connects InfoNCE to MI estimation.

²In the sense that they do not render closed-form expressions.

³Formally, $I(X; Y) = H(X) - H(X|Y) = H(Y) - H(Y|X)$, where $H(X)$ (resp. $H(X|Y)$) denotes the Shannon entropy (resp. conditional Shannon entropy) of a random variable.

⁴This is technically equivalent to the original definition due to the symmetry of K samples.

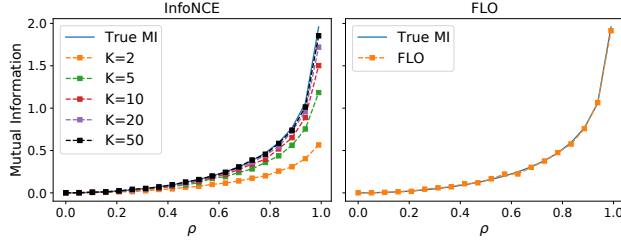


Figure 2: Comparison of InfoNCE and FLO bounds.

Algorithm 1 FLO

Empirical data $\hat{p}_d = \{(x_i, y_i)\}_{i=1}^n$
Model parameters $\Psi = (\theta, \phi)$
for $t = 1, 2, \dots$ **do**
 Sample $i, i' \sim [n]$
 $u = u_\phi(x_i), g_\oplus = g_\theta(x_i, y_i),$
 $g_\ominus = g_\theta(x_i, y_{i'})$
 $\mathcal{F} = u + \exp(-u + g_\ominus - g_\oplus)$
 $\Psi_t = \Psi_t - \eta_t \nabla_{\Psi} \mathcal{F}$
end for

Proposition 2.1. InfoNCE is an asymptotically tight lower bound to the mutual information, *i.e.*

$$I(X; Y) \geq I_{\text{InfoNCE}}^K(X; Y|f), \quad \lim_{K \rightarrow \infty} I_{\text{InfoNCE}}^K(X; Y) \rightarrow I(X; Y). \quad (6)$$

Fenchel-Legendre duality A key idea we exploit is to use the convex duality for converting MI estimators. Let $f(t)$ be a proper convex, lower-semicontinuous function; then its convex conjugate function $f^*(v)$ is defined as $f^*(v) = \sup_{t \in \mathcal{D}(f)} \{tv - f(t)\}$, where $\mathcal{D}(f)$ denotes the domain of function f [48]. We call $f^*(v)$ the *Fenchel conjugate* of $f(t)$, which is again convex and lower-semicontinuous. In physics, this is more commonly known as the *Legendre transformation*, where functions of one quantity (*e.g.*, position, pressure, temperature) are converted into functions of its conjugate quantity (*e.g.*, momentum, volume, entropy, respectively). The Fenchel conjugate pair (f, f^*) are dual to each other, in the sense that $f^{**} = f$, *i.e.*, $f(t) = \sup_{v \in \mathcal{D}(f^*)} \{vt - f^*(v)\}$. As a concrete example, $(-\log(t), -1 - \log(-v))$ gives such a pair, which we exploit in the next section.

2.2 Fenchel-Legendre Optimization for mutual information estimation

With the above mathematical tools, we are ready to present the main result of this paper. To make the derivation more intuitive, and expose a direct connection to the multi-sample estimators, we will show how to get our new estimator from InfoNCE. See the Appendix for alternative derivations.

The naïve Fenchel-Legendre formulation. Our key insight is that MI estimation is essentially an unnormalized statistical model, which can be efficiently handled by the Fenchel-Legendre transform technique. Specifically, the Fenchel-Legendre dual expression of $-\log(t)$ is given by

$$-\log(t) = \max_u \{-u - \exp(-u)t + 1\} = -\min_u \{u + \exp(-u)t\} + 1. \quad (7)$$

Now consider the InfoNCE estimator (5). By denoting $g(x, y) \triangleq \log f(x, y)$, we can rewrite the InfoNCE estimator as

$$I_{\text{InfoNCE}}^K(X; Y) = \mathbb{E}_{p^K(x, y)} \left[\underbrace{-\log \frac{1}{K} \sum_{k'} \exp(g(x_1, y_{k'}) - g(x_1, y_1))}_{\text{Contrast}} \right]. \quad (8)$$

$I_K(\{(x_k, y_k)\})$

Applying (7) to the above equation gives us the following *naïve Fenchel-Legendre* (NFL) bound

$$I_K(\{(x_k, y_k)\}) = -\min_u \left\{ u + \frac{1}{K} \sum_{k'} \exp(-u + g(x_1, y_{k'}) - g(x_1, y_1)) \right\} + 1 \triangleq I_{\text{NFL}}^K. \quad (9)$$

This bound may be unappealing at first sight, for a number of reasons: (i) it is looser than InfoNCE; (ii) u is a function of K -pairs of inputs, which complicates implementation; (iii) the nested optimization for u makes training more costly; (iv) exponentiation of the positive-negative contrasts amplifies the variance issue. Nonetheless, as we shall show, with slight modifications, these issues can be readily fixed.

The improved FLO. To make our implementation easier, we take $K \rightarrow \infty$, and then the summation converges to the expectation respect to the base measure $\mu(y) = p(y)$, *i.e.*,

$$\lim_{K \rightarrow \infty} \left\{ \frac{1}{K} \sum_{k'} \exp(g(x_1, y_{k'}) - g(x_1, y_1)) \right\} = \mathbb{E}_{p(y')} [\exp(g(x_1, y') - g(x_1, y_1))]. \quad (10)$$

This has an important implication: in the asymptotic limit, u can be drastically simplified, thus allowing definition of the single-sample *Fenchel-Legendre Optimization* (FLO) estimator

$$I_{\text{FLO}}(X; Y|u, g) \triangleq -\mathbb{E}_{p(x, y)p(y')} [u(x, y) + \exp(-u(x, y) + g(x, y') - g(x, y))] + 1, \quad (11)$$

$$I_{\text{FLO}}(X; Y) \triangleq \max_{u, g} \{I_{\text{FLO}}(X; Y|u, g)\}, \quad (12)$$

where we identify y' as the *negative* sample. We present the pseudo-code for FLO in Algorithm 1.

To better understand FLO, we wish to know what is the auxiliary function $u(x, y)$ actually learning. Recall in UBA, the optimal critic that gives the tight MI estimate is given by $g^*(x, y) = \log p(x|y) + c(x)$, where $c(x)$ can be an arbitrary function of x [49]. Note this $g^*(x, y)$ is not directly interpretable, however, by fixing (x, y) and integrating out $p(y')$ with respect to this $g^*(x, y)$, we have

$$\mathbb{E}_{p(y')} [\exp(g^*(x, y') - g^*(x, y))] = \frac{p(x)}{p(x|y)} = \frac{p(x)p(y)}{p(x, y)}, \quad (13)$$

the likelihood ratio between the marginals and joint. On the other hand, for fixed $g(x, y)$, $u(x, y)$ attains its optimal value when $u^*(x, y) = \log \mathbb{E}_{p(y')} [\exp(g(x, y') - g(x, y))]$, and together we have

$$u^*(x, y; g^*) = -\log \frac{p(x, y)}{p(x)p(y)}. \quad (14)$$

This proves $u(x, y)$ learns the negative *point-wise mutual information* (PMI).

Note that while $g^*(x, y)$ is not directly meaningful, because of the arbitrary drift term $c(x)$, in FLO we have $u^*(x, y)$ to correct it and recover the PMI. This shows $u(x, y)$ enjoys the nice *self-normalizing* property. It also implies more compact parameterization: since $u^*(x, y) = -g^*(x, y) + c(x) - \log p(x)$, we can parameterize $u_\phi(x, y)$ with $u_\phi(x, y) = -g_\theta(x, y) + s_\psi(x)$, where $\phi = (\theta, \psi)$. This modeling choice imposes structural constraints on the parameterization of (g_θ, u_ϕ) that respect the optimality condition.

Practical implementations. To enable efficient knowledge transfer between similar samples, we amortize the learning of the critic $g(x, y)$ and PMI $u(x, y)$ through neural networks $u_\phi(x, y)$ and $g_\theta(x, y)$. We note that efficient parameter sharing can be achieved by modeling $u_\phi(x, y)$ and $g_\theta(x, y)$ jointly with a single neural network $f_\psi(x, y) : \mathcal{X} \times \mathcal{Y} \rightarrow \mathbb{R}^2$ with two output heads, *i.e.*, $[u_i, g_i] = f_\psi(x_i, y_i)$. Consequently, although FLO has an additional target u_ϕ relative to its single-critic counterparts, such as InfoNCE, it does not actually induce extra modeling cost. In fact, this shared parameterization promotes synergy between the two learners for better sample efficiency.

To further enhance computation efficiency, we consider *bi-linear* critic functions. In particular, let $g_\theta(x, y) = \langle h_\theta(x), \tilde{h}(y) \rangle / \tau$, where $h : \mathcal{X} \rightarrow \mathbb{S}^p$ and $\tilde{h} : \mathcal{Y} \rightarrow \mathbb{S}^p$ respectively map x and y to a shared unit sphere \mathbb{S}^p embedded in \mathbb{R}^{p+1} , $\langle a, b \rangle = a^T b$ is the inner product operation, and $\tau > 0$ is the temperature parameter. Thus the evaluation of the *Gram* matrix $G = h(\mathbb{X})^T \tilde{h}(\mathbb{Y}) / \tau$, where $[\mathbb{X}, \mathbb{Y}] \in \mathbb{R}^{K \times (d_x + d_y)}$ is a mini-batch of K -paired samples and $g_\theta(x_i, y_j) = G_{ij}$, can be massively parallelized via matrix multiplication. In this setup, the diagonal terms of G are from positive samples while the off-diagonal terms are from negative samples. A similar approach has been widely employed in the contrastive representation learning literature (*e.g.*, SimCLR [11]), where the major conceptual difference is that these works consider h, \tilde{h} directly as the feature encoders, and consequently encouraging a flattened representations by design. For applications where more compact summaries of representation are desired, one will need to decouple the encoder and the contrast critic(s).

2.3 Connections to the existing MI bounds

Due to space limitations, we elaborate the connections to the existing MI bounds here, and have relegated an extended related work discussion in a broader context to the Appendix.

From log-partition approximation to MI bounds. To embrace a more holistic understanding, we summarize popular variational MI bounds in Table 1, along with FLO and its variants. With the exception of JSD, we can view the difference of these variational bounds from the perspective of unnormalized statistical modeling, as they differ in how the log partition function $\log Z(x)$ is estimated. We can broadly categorize these estimators into two families: the log-family (DV, MINE, InfoNCE) and the exponential-family (NWJ, TUBA, FLO). In the log-family, DV and InfoNCE are multi-sample estimators that leverage direct Monte-Carlo estimates \hat{Z} for $\log Z(x)$, and these two differ in whether to include the positive sample in the denominator or not. To avoid the excessive computation and memory usage incurred by the in-batch computation of the normalizer, MINE further employed *exponential moving average* (EMA) to aggregate normalizer across batches. Note for the log-family estimators, their variational gaps are partly caused by the log-transformation on finite-sample average due to Jensen’s inequality (*i.e.*, $\log Z = \log \mathbb{E}[\hat{Z}] \leq \mathbb{E}[\log \hat{Z}]$). In contrast,

Table 1: Comparison of popular variational MI estimators. Here $g(x, y)$, $u(x, y)$ and $u(x)$ are variational functions to be optimized, $\sigma(u) = \frac{1}{1+\exp(-u)}$ is the Sigmoid function, $\mathcal{E}[f(u), \eta]$ denotes exponential average of function $f(u)$ with decay parameter $\eta \in (0, 1)$, and $\alpha \in [0, 1]$ is the balancing parameter trading off bias and variance btw InfoNCE and TUBA. To highlight the contrastive view, we use (x, p_\oplus) to denote samples drawn from the joint density $p(x, y)$, and (x, y_\ominus) to denote samples drawn from the product of marginal $p(x)p(y)$. In context, y_\oplus and y_\ominus enjoy the intuitive interpretation of positive and negative samples. We exclude variational upper bounds here because their computation typically involves the explicit knowledge of conditional likelihoods.

Name	Objective	Bias	Var.
DV [30]	$g(x, y_\oplus) - \log(\sum_{k=1}^K \exp(g(x^k, y_\ominus^k)) / K)$	large	high
MINE [50]	$g(x, y_\oplus) - \log(\mathcal{E}[\exp(g(x, y_\ominus)), \eta])$	low	high
NWJ [31]	$g(x, y_\oplus) - \exp(g(x, y_\ominus) - 1)$	low	high
JSD [23]	$g^*(x, y_\oplus) - \exp(g^*(x, y_\ominus) - 1)$	low	high
	$g^* \leftarrow \arg \max \{ \log \sigma(g(x, y_\oplus)) + \log \sigma(-g(x, y_\ominus)) \}$		
TUBA [28]	$g(x, y_\oplus) + u(x) + 1 - \exp(g(x, y_\ominus) - u(x))$	low	high
$m_{\alpha, u}(x, y^{1:K}) \triangleq \alpha \frac{1}{K} \left\{ \sum_{k=1}^K \exp(g(x, y^k)) \right\} + (1 - \alpha) \exp(u(x)), m(\cdot) \triangleq m_{0, u}(\cdot)$			
InfoNCE [9]	$g(x, y_\oplus) - \log(m(x, \{y_\oplus, y_\ominus^{1:K-1}\}))$	large	low
α -InfoNCE [28]	$g(x, y_\oplus) - g(x, y_\ominus) - \log(m_{\alpha, u}(x, \{y_\oplus, y_\ominus^{1:K-1}\}))$ $+ \log(m_{\alpha, u}(x, y_\ominus^{1:K}))$	flex	flex
FLO (ours)	$u(x, y_\oplus) + \exp(-u(x, y_\oplus) + g(x, y_\ominus) - g(x, y_\oplus))$	low	high

the objective of exponential-family estimators do not involve such log-transformation, since they can all be derived from the Fenchel-Legendre inequality: NWJ directly applies the Fenchel dual of f -divergence for MI [51], while TUBA exploits this inequality to compute the log partition function $\log Z(x) = \log \mathbb{E}_\ominus[\exp(g(x, y_\ominus))]$. Motivated from a contrastive viewpoint, our FLO applies the Fenchel-Legendre inequality to the log-partition of contrast scores.

The contrastive view for MI estimation. The MI estimators can also be categorized based on how they contrast the samples. For instance, NWJ and TUBA are generally considered to be non-contrastive estimators, as their objectives do not compare positive sample against negative samples on the same scale (*i.e.*, log versus exp), and this might explain their lack of effectiveness in representation learning applications. For JSD, it depends on a two-stage estimation procedure similar to that in adversarial training to assess the MI, by explicitly contrasting positive and negative samples to estimate the likelihood ratio. This strategy has been reported to be unstable in many empirical settings. The log-family estimators can be considered as a multi-sample, single-stage generalization of JSD. However, the DV objective can go unbounded thus resulting in a large variance, and the contrastive signal is decoupled by the EMA operation in MINE. Designed from contrastive perspectives, InfoNCE trades bound tightness for a lower estimation variance, which is found to be crucial in representation learning applications. Our FLO formalizes the contrastive view for exponential-family MI estimation, and nicely bridges existing bounds: the PMI normalizer $\exp(-u(x, y))$ is a more principled treatment than the EMA in MINE, and compared to DV the positive and negative samples are explicitly contrasted and adaptively normalized.

Important FLO variants. We now demonstrate that FLO is a flexible framework that not only recovers existing bounds, but also derives new ones. Recall the optimal $u^*(x, y)$ given $g_\theta(x, y)$ is in the form of $-g_\theta(x, y) + s_\psi(x)$, and parameterizing $u(x, y)$ in this way recovers the TUBA bound. We make two important remarks: (i) fixing either of u and g , and optimizing with respect to the other also gives a valid lower bound to MI; and (ii) a carefully chosen multi-input $u(\{(x_i, y_i)\})$ can be computationally appealing. As a concrete example, if we set u_ϕ to

$$u_\phi(\{(x_i, y_i)\}) = \log \left(\frac{1}{K} \sum_j \exp(g_\theta(x_i, y_j) - g_\theta(x_i, y_i)) \right) \quad (15)$$

and update $u_\theta(x, y)$ while artificially keeping $g_\theta(x, y)$ fixed⁵, then FLO falls back to DV. Alternatively, we can consider the Fenchel dual version of it: using the same multi-input $u_\phi(\{x_i, y_i\})$ in (15), treat u_ϕ as fixed and only update g_θ , and this gives us the following novel MI objective we call *Fenchel-Donsker-Varadhan* (FDV) estimator:

$$I_{\text{FDV}} \triangleq \hat{I}_{\text{DV}}(\{(x_i, y_i)\}) + \frac{\sum_j \exp(g_\theta(x_i, y_j) - g_\theta(x_i, y_i))}{\sum_j \exp(\hat{g}_\theta(x_i, y_j) - \hat{g}_\theta(x_i, y_i))} - 1, \quad (16)$$

where we have used \hat{g}, \hat{I} to denote evaluation-only mode for the corresponding functions (because they are the “fixed” u_ϕ and do not backpropagate parameter gradients).

2.4 Theory of FLO

In this section, we show the proposed FLO enjoys appealing theoretical properties, making it an attractive candidate for MI estimation and optimization. Based on our analysis from the previous sections, the following results are immediate.

Proposition 2.2. The FLO estimator is tight

$$I(X; Y) = -\min_{u, g} \{ \mathbb{E}_{p(x, y)p(y')} [u(X, Y) + \exp(-u(X, Y) + g(X, Y') - g(X, Y))] \} + 1 \quad (17)$$

Corollary 2.3. Let $u^*(x, y)$ be the solution for (17), then we have

$$I(X, Y) = \mathbb{E}_{p(x, y)}[-u^*(X, Y)]. \quad (18)$$

Gradient and convergence analyses of FLO To further our understanding of FLO, we examine its parameter gradients. Recall the intractable UBA bound can be re-expressed as:

$$I_{\text{UBA}}(g_\theta) = \mathbb{E}_{p(x, y)}[-\log \mathbb{E}_{p(y')}[\exp(g_\theta(x, y') - g_\theta(x, y))]] \quad (19)$$

We want to establish the intuition that $\nabla_\theta \{I_{\text{FLO}}(u_\phi, g_\theta)\} \approx \nabla_\theta \{I_{\text{UBA}}(g_\theta)\}$, where

$$I_{\text{FLO}}(u_\phi, g_\theta) \triangleq -\{u_\phi(x, y) + \mathbb{E}_{p(y')}[\exp(-u_\phi(x, y) + g_\theta(x, y') - g_\theta(x, y))]\} \quad (20)$$

is our FLO estimator. Denoting the integral by $\mathcal{E}_\theta(x, y) \triangleq \frac{1}{\mathbb{E}_{p(y')}[\exp(g_\theta(x, y') - g_\theta(x, y))]}$, we have

$$\mathbb{E}_{p(y')}[\nabla_\theta \{\exp(g_\theta(x, y') - g_\theta(x, y))\}] = \nabla_\theta \left\{ \frac{1}{\mathcal{E}_\theta(x, y)} \right\} = -\frac{\nabla_\theta \log \mathcal{E}_\theta(x, y)}{(\mathcal{E}_\theta(x, y))^2} = -\frac{\nabla_\theta \log \mathcal{E}_\theta(x, y)}{\mathcal{E}_\theta(x, y)}. \quad (21)$$

Since for fixed $g_\theta(x, y)$ the corresponding optimal $u_\theta^*(x, y)$ maximizing FLO is given by

$$u_\theta^*(x, y) = \log \mathbb{E}_{p(y')}[\exp(g_\theta(x, y') - g_\theta(x, y))] = -\log \mathcal{E}_\theta(x, y), \quad (22)$$

this relation implies the term $\exp^{-u_\phi(x, y)}$ is essentially optimized to approximate $\mathcal{E}_\theta(x, y)$. To emphasize this point, we now write $\hat{\mathcal{E}}_\theta(x, y) \triangleq e^{-u_\phi(x, y)}$. When this approximation is sufficiently accurate (i.e., $\mathcal{E}_\theta \approx \hat{\mathcal{E}}_\theta$), we can show ∇I_{FLO} approximates ∇I_{UBA} as follows

$$\nabla_\theta \{I_{\text{FLO}}(u_\phi, g_\theta)\} = -\mathbb{E}_{p(x, y)} \left[e^{-u_\phi(x, y)} \mathbb{E}_{p(y')}[\nabla_\theta \exp(g_\theta(x, y') - g_\theta(x, y))] \right] \quad (23)$$

$$= \mathbb{E}_{p(x, y)} \left[\frac{\hat{\mathcal{E}}_\theta(x, y)}{\mathcal{E}_\theta(x, y)} \nabla_\theta \log \mathcal{E}_\theta(x, y) \right] \approx \mathbb{E}_{p(x, y)} [\nabla_\theta \log \mathcal{E}_\theta(x, y)] \quad (24)$$

$$= \nabla_\theta \{ \mathbb{E}_{p(x, y)}[\log \mathcal{E}_\theta(x, y)] \} = \nabla_\theta \{I_{\text{UBA}}(g_\theta)\}. \quad (25)$$

Indeed, we can prove FLO converges under much weaker conditions, even when this approximation $\hat{u}(x, y)$ is very rough. The intuition is simple: in (24), the term $\frac{\hat{\mathcal{E}}_\theta}{\mathcal{E}_\theta}$ only rescales the gradient, which implies the optimizer will still proceed in the right direction. The informal version of our result is summarized in the Proposition below (see the Appendix for the formal version and proof).

Proposition 2.4 (Convergence of FLO, informal version). Let $\{\eta_t\}_{t=1}^\infty$ be the stochastic *Robbins-Monro* sequence of learning rate: $\sum_t \mathbb{E}[\eta_t] = \infty$ and $\sum_t \mathbb{E}[\eta_t^2] < \infty$. If $\frac{\hat{\mathcal{E}}_\theta}{\mathcal{E}_\theta}$ is bounded between $[a, b]$ ($0 < a < b < \infty$), then under the stochastic gradient descent scheme described in Algorithm 1, θ_t converges to a stationary point of $I_{\text{UBA}}(g_\theta)$ with probability 1, i.e., $\lim_{t \rightarrow \infty} \|\nabla I_{\text{UBA}}(g_{\theta_t})\| = 0$. Additionally assume I_{UBA} is convex with respect to θ , then FLO converges with probability 1 to the global optimum θ^* of I_{UBA} from any initial point θ_0 .

⁵That is to say g_θ in u_ϕ is an independent copy of g_θ .

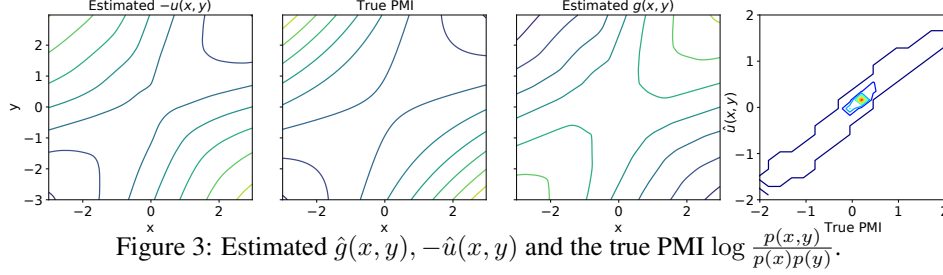


Figure 3: Estimated $\hat{g}(x, y)$, $-\hat{u}(x, y)$ and the true PMI $\log \frac{p(x, y)}{p(x)p(y)}$.

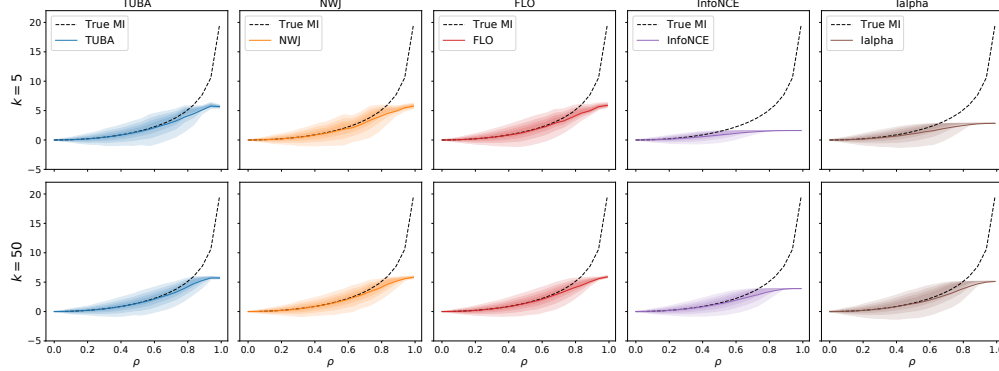


Figure 4: Bias variance plot for the popular MI bounds with the 10-D Gaussians.

3 Experiments

We consider a wide range of tasks to validate FLO and benchmark it against state-of-the-art solutions. Details of experimental setups are described the Appendix, and our code is available from <https://github.com/qingguo666/FLO>. All experiments are implemented with PyTorch.

Toy model. Following [28], we use the toy models described below in our experiments. The $2d$ -dimensional Gaussian $(X, Y) \in \mathbb{R}^d \times \mathbb{R}^d$, where each paired $[(x^i, y^i)]_{i=1}^d$ are correlated 2-dimensional Gaussians with correlation parameter ρ , and samples are independent with $i \neq j$. The ground-truth MI is then given by $-\frac{d}{2} \cdot \log(1 - \rho^2)$. To verify our theoretical predictions, in Figure 2 we compare the single-sample FLO to the ground-truth MI and its multi-sample counterpart InfoNCE. And in Figure 3, we plot the estimated $\hat{g}(x, y)$, $\hat{u}(x, y)$ along with the ground-truth PMI function.

Comparison to baseline MI bounds. In Figure 4 we compare FLO to the following baseline estimators: NWJ, TUBA, InfoNCE and α - InfoNCE. To make our comparisons fair, we implemented the multi-sample version of all estimators, such that all models are running on the same negative-sample budget ($K \in \{5, 50\}$). This is in contrast to the results from prior literature where the multi-sample InfoNCE was compared to the single-sample version of its counterparts. We note the DV estimator did not report reasonable results for the negative sample budget we consider here⁶, so it was excluded from our analyses. We report $\alpha = 0.8$ here for the α -InfoNCE.

We consider $d = 10$ and $\rho \in [0, 0.99]$ here, which provides a reasonable coverage of the range of MI one may encounter in empirical settings. To focus on the bias-variance trade-offs, we plot the decimal quantiles in addition to the estimated MI. While confirming the folklore that the InfoNCE-family bounds are more stable albeit more biased, contrary to what one might intuitively expect, we notice their variance actually increased after we bumped up the negative sample budget, while all other bounds have their variance reduced. The reason is with more negative samples, the MI bound is tighter and consequently the fundamental law of estimation variance kicks in [33]. Whereas for fixed MI, the variance decreases with increasing sample budget [28]. This means the low variance argument supporting InfoNCE’s superior empirical performance stands to be challenged, as we see growth of both bound and variance with a large K . With larger MI values where the bounds have severely underestimated, we also see small estimation variance since the critic functions have been saturated. All non-InfoNCE bounds, including FLO, perform similarly.

Model parameterization. Now we want to show how different parameterization schemes affect the performance and learning efficiency for FLO. In Figure 5, we visualize the learning dynamics of FLO

⁶It works only with an excessively large K .

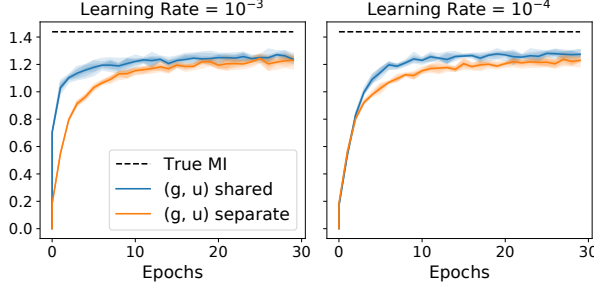


Figure 5: Comparison of shared and separate parameterization for (g_θ, u_ϕ) . Single-network parameterization not only runs faster but also learns more efficiently.

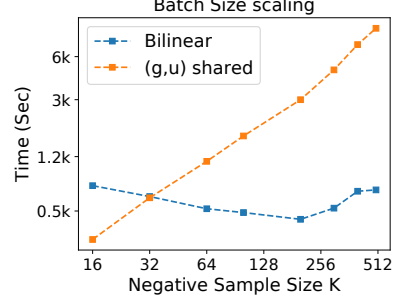


Figure 6: Comparison of computation time of joint MLP critic and bi-linear critic.

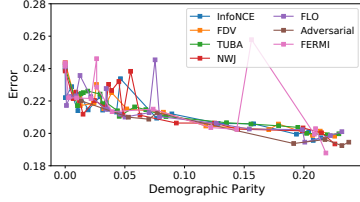


Figure 7: Fair Learning Result.

using a shared network for (g_θ, u_ϕ) and that with two separate networks. The parameter sharing not only cuts computations, it also helps to learn faster. There is no discernible difference in performance and FLO-separate used twice much of iterations to converge. Next, we compare the bi-linear critic implementation (FLO-BiL) to the standard MLP with paired inputs (x, y) (Figure 6). In the bi-linear case K is tied to batch-size so we scale the computation budget with $T(K) = (\frac{K}{K_0})^{\frac{1}{2}} \cdot T_0$, where (T_0, K_0) are respectively the baseline training iteration and negative sample size used by FLO-MLP. We see FLO-BiL has drastically reduced computations (Figure 6).

Cross-view representation learning. In our last experiment, we want to show the proposed FLO and its variant can be used for representation learning. In this experiment, we cut MNIST images in the middle to split into the left and right halves $(x_l$ and x_r). Our goal is to find low dimensional features (e.g., $d = 5$) that maximally encode the information for the other half. To evaluate the utility of the extracted representations, we concatenated the features from the respective halves and use it for the prediction of image labels, using a three layer neural network. Our results are summarized in Table 2. The linear *canonical correlation analysis* (CCA) gives the worst performance. The NWJ estimator give the highest MI estimate, yet it under-performs all other MI-based losses. While TUBA outperforms the original FLO, it is superseded by the FDV estimator.

Classification with sensitive attributes. Next we demonstrate FLO’s utility in building fair machine learning models [52]. In this setting, we have an additional sensitive attribute s associated with each data point, which encodes potential bias during data collection, and our goal is to build a bia-free predictor. Following [53], we optimize the regularized objective,

$$\mathcal{L} = \underbrace{\text{Loss}(\text{Predictor}(\text{Encoder}(x_i)), y_i)}_{\text{Primary loss}} + \lambda \underbrace{I(s_i, \text{Encoder}(x_i))}_{\text{Debiasing}}. \quad (26)$$

where we use different MI estimators for the sensitive regularization. In Figure 7, we compare our MI-estimator based fair learning models with state-of-the-art solutions such as *adversarial debiasing* [54] and *FERMI* [55] on the *adult* dataset, our MI-based solutions perform strongly and robustly.

4 Conclusion

In this research, we have described a new framework for the contrastive estimation of mutual information from energy modeling perspectives. Our work not only encapsulates popular variational MI bounds but also inspires novel objectives such as FLO and FDV, which comes with strong theoretical guarantees. In future work, we seek to leverage our theoretical insights to improve practical applications involving MI estimation, such as representation learning and algorithmic fairness.

References

- [1] D. N. Reshef, Y. A. Reshef, H. K. Finucane, S. R. Grossman, G. McVean, P. J. Turnbaugh, E. S. Lander, M. Mitzenmacher, and P. C. Sabeti, “Detecting novel associations in large data sets,” *science*, vol. 334, no. 6062, pp. 1518–1524, 2011.
- [2] C. E. Shannon, “A mathematical theory of communication,” *The Bell system technical journal*, vol. 27, no. 3, pp. 379–423, 1948.
- [3] D. J. MacKay, *Information theory, inference and learning algorithms*. Cambridge university press, 2003.
- [4] F. R. Bach and M. I. Jordan, “Kernel independent component analysis,” *Journal of Machine Learning Research*, vol. 3, no. Jul, pp. 1–48, 2002.
- [5] U. Gupta, A. Ferber, B. Dilkina, and G. V. Steeg, “Controllable guarantees for fair outcomes via contrastive information estimation,” *arXiv preprint arXiv:2101.04108*, 2021.
- [6] S. E. Palmer, O. Marre, M. J. Berry, and W. Bialek, “Predictive information in a sensory population,” *Proceedings of the National Academy of Sciences*, vol. 112, no. 22, pp. 6908–6913, 2015.
- [7] S. Kleinegesse and M. U. Gutmann, “Bayesian experimental design for implicit models by mutual information neural estimation,” in *ICML, PMLR*, 2020.
- [8] N. Tishby and N. Zaslavsky, “Deep learning and the information bottleneck principle,” in *2015 IEEE Information Theory Workshop (ITW)*, pp. 1–5, IEEE, 2015.
- [9] A. v. d. Oord, Y. Li, and O. Vinyals, “Representation learning with contrastive predictive coding,” *arXiv preprint arXiv:1807.03748*, 2018.
- [10] K. He, H. Fan, Y. Wu, S. Xie, and R. Girshick, “Momentum contrast for unsupervised visual representation learning,” in *CVPR*, 2020.
- [11] T. Chen, S. Kornblith, M. Norouzi, and G. Hinton, “A simple framework for contrastive learning of visual representations,” in *ICML*, 2020.
- [12] J.-B. Grill, F. Strub, F. Altché, C. Tallec, P. H. Richemond, E. Buchatskaya, C. Doersch, B. A. Pires, Z. D. Guo, M. G. Azar, *et al.*, “Bootstrap your own latent: A new approach to self-supervised learning,” in *NeurIPS*, 2020.
- [13] R. Battiti, “Using mutual information for selecting features in supervised neural net learning,” *IEEE Transactions on neural networks*, vol. 5, no. 4, pp. 537–550, 1994.
- [14] F. Maes, A. Collignon, D. Vandermeulen, G. Marchal, and P. Suetens, “Multimodality image registration by maximization of mutual information,” *IEEE transactions on Medical Imaging*, vol. 16, no. 2, pp. 187–198, 1997.
- [15] L. Paninski, “Estimation of entropy and mutual information,” *Neural computation*, vol. 15, no. 6, pp. 1191–1253, 2003.
- [16] J. P. Pluim, J. A. Maintz, and M. A. Viergever, “Mutual-information-based registration of medical images: a survey,” *IEEE transactions on medical imaging*, vol. 22, no. 8, pp. 986–1004, 2003.
- [17] K. Torkkola, “Feature extraction by non-parametric mutual information maximization,” *Journal of machine learning research*, 2003.
- [18] A. Kraskov, H. Stögbauer, and P. Grassberger, “Estimating mutual information,” *Physical review E*, vol. 69, no. 6, p. 066138, 2004.
- [19] F. Pérez-Cruz, “Estimation of information theoretic measures for continuous random variables,” in *NIPS*, 2008.
- [20] S. Gao, G. Ver Steeg, and A. Galstyan, “Efficient estimation of mutual information for strongly dependent variables,” in *AISTATS, PMLR*, 2015.
- [21] A. Gretton, R. Herbrich, and A. J. Smola, “The kernel mutual information,” in *ICASSP*, 2003.
- [22] A. Gretton, R. Herbrich, A. Smola, O. Bousquet, B. Schölkopf, *et al.*, “Kernel methods for measuring independence,” *Journal of Machine Learning Research*, 2005.

- [23] R. D. Hjelm, A. Fedorov, S. Lavoie-Marchildon, K. Grewal, P. Bachman, A. Trischler, and Y. Bengio, “Learning deep representations by mutual information estimation and maximization,” in *ICLR*, 2019.
- [24] T. Suzuki, M. Sugiyama, J. Sese, and T. Kanamori, “Approximating mutual information by maximum likelihood density ratio estimation,” in *New challenges for feature selection in data mining and knowledge discovery*, pp. 5–20, PMLR, 2008.
- [25] M. Arjovsky and L. Bottou, “Towards principled methods for training generative adversarial networks,” in *ICLR*, 2017.
- [26] Y. Bengio, A. Courville, and P. Vincent, “Representation learning: A review and new perspectives,” *IEEE transactions on pattern analysis and machine intelligence*, vol. 35, no. 8, pp. 1798–1828, 2013.
- [27] L. Wen, Y. Zhou, L. He, M. Zhou, and Z. Xu, “Mutual information gradient estimation for representation learning,” in *ICLR*, 2020.
- [28] B. Poole, S. Ozair, A. Van Den Oord, A. Alemi, and G. Tucker, “On variational bounds of mutual information,” in *ICML*, PMLR, 2019.
- [29] D. Barber and F. Agakov, “The IM algorithm: a variational approach to information maximization,” *NIPS*, vol. 16, p. 201, 2004.
- [30] M. D. Donsker and S. S. Varadhan, “Asymptotic evaluation of certain markov process expectations for large time. iv,” *Communications on Pure and Applied Mathematics*, vol. 36, no. 2, pp. 183–212, 1983.
- [31] X. Nguyen, M. J. Wainwright, and M. I. Jordan, “Estimating divergence functionals and the likelihood ratio by convex risk minimization,” *IEEE Transactions on Information Theory*, vol. 56, no. 11, pp. 5847–5861, 2010.
- [32] A. Alemi, B. Poole, I. Fischer, J. Dillon, R. A. Saurous, and K. Murphy, “Fixing a broken ELBO,” in *ICML*, pp. 159–168, 2018.
- [33] D. McAllester and K. Stratos, “Formal limitations on the measurement of mutual information,” *arXiv preprint arXiv:1811.04251*, 2018.
- [34] J. Song and S. Ermon, “Understanding the limitations of variational mutual information estimators,” in *ICLR*, 2020.
- [35] M. Gutmann and A. Hyvärinen, “Noise-contrastive estimation: A new estimation principle for unnormalized statistical models,” in *AISTATS*, 2010.
- [36] A. Mnih and K. Kavukcuoglu, “Learning word embeddings efficiently with noise-contrastive estimation,” in *NIPS*, 2013.
- [37] Z. Wu, Y. Xiong, S. X. Yu, and D. Lin, “Unsupervised feature learning via non-parametric instance discrimination,” in *CVPR*, pp. 3733–3742, 2018.
- [38] Y. Tian, D. Krishnan, and P. Isola, “Contrastive multiview coding,” *arXiv preprint arXiv:1906.05849*, 2019.
- [39] A. Radford, J. W. Kim, C. Hallacy, A. Ramesh, G. Goh, S. Agarwal, G. Sastry, A. Askell, P. Mishkin, J. Clark, *et al.*, “Learning transferable visual models from natural language supervision,” *arXiv preprint arXiv:2103.00020*, 2021.
- [40] R. Linsker, “Self-organization in a perceptual network,” *Computer*, vol. 21, no. 3, pp. 105–117, 1988.
- [41] R. Shwartz-Ziv and N. Tishby, “Opening the black box of deep neural networks via information,” *arXiv preprint arXiv:1703.00810*, 2017.
- [42] M. Tschannen, J. Djolonga, P. K. Rubenstein, S. Gelly, and M. Lucic, “On mutual information maximization for representation learning,” *ICLR*, 2020.
- [43] C. Tao, L. Chen, S. Dai, J. Chen, K. Bai, D. Wang, J. Feng, W. Lu, G. Bobashev, and L. Carin, “On fenchel mini-max learning,” in *NeurIPS*, 2019.
- [44] J. O. Berger, *Statistical decision theory and Bayesian analysis*. Springer Science & Business Media, 2013.
- [45] L. E. Reichl, *A modern course in statistical physics*. John Wiley & Sons, 2016.
- [46] D. Barber and F. V. Agakov, “Information maximization in noisy channels: A variational approach,” *NIPS*, vol. 16, 2003.

- [47] A. Grover and J. Leskovec, “node2vec: Scalable feature learning for networks,” in *SIGKDD*, 2016.
- [48] J.-B. Hiriart-Urruty and C. Lemaréchal, *Fundamentals of convex analysis*. Springer Science & Business Media, 2012.
- [49] Z. Ma and M. Collins, “Noise contrastive estimation and negative sampling for conditional models: Consistency and statistical efficiency,” *arXiv preprint arXiv:1809.01812*, 2018.
- [50] M. I. Belghazi, A. Baratin, S. Rajeshwar, S. Ozair, Y. Bengio, A. Courville, and D. Hjelm, “Mutual information neural estimation,” in *ICML*, PMLR, 2018.
- [51] S. Nowozin, B. Cseke, and R. Tomioka, “f-GAN: Training generative neural samplers using variational divergence minimization,” in *NIPS*, 2016.
- [52] C. Dwork, M. Hardt, T. Pitassi, O. Reingold, and R. Zemel, “Fairness through awareness,” in *Proceedings of the 3rd innovations in theoretical computer science conference*, 2012.
- [53] J. Song, P. Kalluri, A. Grover, S. Zhao, and S. Ermon, “Learning controllable fair representations,” in *AISTATS*, 2019.
- [54] B. H. Zhang, B. Lemoine, and M. Mitchell, “Mitigating unwanted biases with adversarial learning,” in *Proceedings of the 2018 AAAI/ACM Conference on AI, Ethics, and Society*, pp. 335–340, 2018.
- [55] A. Lowy, R. Pavan, S. Baharlouei, M. Razaviyayn, and A. Beirami, “Fermi: Fair empirical risk minimization via exponential Rényi mutual information,” *arXiv preprint arXiv:2102.12586*, 2021.
- [56] G. Ver Steeg and A. Galstyan, “Information-theoretic measures of influence based on content dynamics,” in *Proceedings of the sixth ACM international conference on Web search and data mining*, pp. 3–12, 2013.
- [57] W. Gao, S. Oh, and P. Viswanath, “Demystifying fixed k -nearest neighbor information estimators,” *IEEE Transactions on Information Theory*, vol. 64, no. 8, pp. 5629–5661, 2018.
- [58] M. Hardt, E. Price, and N. Srebro, “Equality of opportunity in supervised learning,” in *NIPS*, 2016.
- [59] R. K. E. Bellamy, K. Dey, M. Hind, S. C. Hoffman, S. Houde, K. Kannan, P. Lohia, J. Martino, S. Mehta, A. Mojsilovic, S. Nagar, K. N. Ramamurthy, J. Richards, D. Saha, P. Sattigeri, M. Singh, K. R. Varshney, and Y. Zhang, “AI Fairness 360: An extensible toolkit for detecting, understanding, and mitigating unwanted algorithmic bias,” Oct. 2018.
- [60] A. Asuncion and D. Newman, “Uci machine learning repository,” 2007.
- [61] D. P. Kingma and M. Welling, “Auto-encoding variational Bayes,” in *ICLR*, 2014.
- [62] A. A. Alemi, I. Fischer, J. V. Dillon, and K. Murphy, “Deep variational information bottleneck,” in *ICLR*, 2016.

Appendix

Table of Contents

A	Proof of Proposition 2.1 (InfoNCE Properties)	13
B	Proof of Proposition 2.2 (FLO Properties)	15
C	Proof of Corollary 2.3 (MI and $u(x, y)$)	15
D	Gradient Analysis of FLO (More Detailed)	15
E	Proof of Proposition 2.4 (FLO Convergence)	16
F	Gaussian Toy Model Experiments	17
F.1	Choice of baselines	17
F.2	Experimental setups	17
F.3	Additional analyses and results	18
G	Cross-view Representation Learning (Extended Analyses)	20
H	Comparison with Classical MI Estimators	20
I	Regression with Sensitive Attributes (Fair Learning) Experiments	21
I.1	Introduction to fair machine learning	21
I.2	Experiment details and analyses	21
J	Self-supervised Learning	22
K	Estimating MI on Tiny-ImageNet	22

A Proof of Proposition 2.1 (InfoNCE Properties)

Proof. We can bound MI from below using an variational distribution $q(y|x)$ as follows:

$$I(X, Y) = \mathbb{E}_{p(x, y)} \left[\log \frac{p(x, y)}{p(x)p(y)} \right] \quad (27)$$

$$= \mathbb{E}_{p(x, y)} \left[\log \frac{p(y|x)p(x)q(y|x)}{p(x)p(y)q(y|x)} \right] \quad q(y|x) \text{ is the variational distribution} \quad (28)$$

$$= \mathbb{E}_{p(x, y)} \left[\log \frac{q(y|x)}{p(y)} \right] + \mathbb{E}_{p(x)} [\text{KL}(p(y|x) || q(y|x))] \quad (29)$$

$$\geq \mathbb{E}_{p(x, y)} [\log q(y|x) - \log p(y)] \triangleq I_{\text{BA}}(X, Y; q) \quad (30)$$

In sample-based estimation of MI, we do not know the ground-truth marginal density $p(y)$, which makes the above BA bound impractical. However, we can carefully choose an energy-based variational density that “cancels out” $p(y)$:

$$q_f(y|x) = \frac{p(y)}{Z_f(x)} e^{f(x, y)}, \quad Z_f(x) \triangleq \mathbb{E}_{p(y)} [e^{f(x, y)}]. \quad (31)$$

This auxiliary function $f(x, y)$ is known as the tilting function in importance weighting literature. Hereafter, we will refer to it the *critic function* in accordance with the nomenclature used in contrastive

learning literature. The partition function $Z_f(x)$ normalizes this $q(y|x)$. Plugging this $q_f(y|x)$ into I_{BA} yields:

$$I_{\text{BA}}(X, Y; q_f) = \mathbb{E}_{p(x, y)}[f(x, y) + \log(p(y)) - \log(Z_f(x)) - \log p(y)] \quad (32)$$

$$= \mathbb{E}_{p(x, y)}[f(x, y)] - \mathbb{E}_{p(x)}[\log(Z_f(x))] \triangleq I_{\text{UBA}}(X, Y; f) \quad (33)$$

For $x, a > 0$, we have inequality $\log(x) \leq \frac{x}{a} + \log(a) - 1$. By setting $x \leftarrow Z(y)$ and $a \leftarrow e$, we have

$$\log(Z(y)) \leq e^{-1} Z(y). \quad (34)$$

Plugging this result into (33) we recover the celebrated NWJ bound, which lower bounds I_{UBA} :

$$I_{\text{UBA}}(X, Y) \geq \mathbb{E}_{p(x, y)}[f(x, y)] - e^{-1} \mathbb{E}_{p(x)}[Z_f(x)] \triangleq I_{\text{NWJ}}(X, Y; f). \quad (35)$$

When $f(x, y)$ takes the value of

$$f^*(x, y) = 1 + \log \frac{p(x|y)}{p(x)}, \quad (36)$$

this bound is sharp.

We next extend these bounds to the multi-sample setting. In this setup, we are given one paired sample (x_1, y_1) from $p(x, y)$ (*i.e.*, the positive sample) and $K - 1$ samples independently drawn from $p(y)$ (*i.e.*, the negative samples). Note that when we average over x wrt $p(x)$ to compute the MI, this equivalent to comparing positive pairs from $p(x, y)$ and negative pairs artificially constructed by $p(x)p(y)$. By the independence between X_1 and $Y_{k>1}$, we have

$$I(X; Y_{1:K}) = \mathbb{E}_{p(x_1, y_1) \prod_{k>1} p(y_k)} \left[\frac{p(x_1, y_1) \prod_{k>1} p(y_k)}{p(x_1) \prod_{k>1} p(y_k)} \right] = \mathbb{E}_{p(x_1, y_1)} \left[\frac{p(x_1, y_1)}{p(x_1)p(y_1)} \right] = I(X; Y) \quad (37)$$

So for arbitrary multi-sample critic $f(x; y_{1:K})$, we know

$$I(X; Y) = I(X_1; Y_{1:K}) \geq I_{\text{NWJ}}(X_1, Y_{1:K}; f) = \mathbb{E}_{p(x_1, y_1) \prod_{k>1} p(y_k)} [f(x_1, y_{1:K})] - e^{-1} \mathbb{E}_{p(x)} [Z_f(x)] \quad (38)$$

Now let us set

$$\tilde{f}(x_1; y_{1:K}) = 1 + \log \frac{e^{g(x_1, y_1)}}{m(x_1; y_{1:K})}, \quad m(x_1; y_{1:K}) = \frac{1}{K} \sum_k e^{g(x_1, y_k)}. \quad (39)$$

$$\begin{aligned} I_{\text{NWJ}}(X_1, Y_{1:K}; \tilde{f}) &= \mathbb{E}_{p(x_1, y_1) p^{K-1}(y_k)} \left[1 + \log \frac{e^{g(x_1, y_1)}}{m(x_1; y_{1:K})} \right] - \mathbb{E}_{p(x') p^K(y')} \left[e^{-1 + 1 + \log \frac{e^{g(x'_1, y'_1)}}{m(x'_1; y'_{1:K})}} \right] \\ &= \mathbb{E}_{p(x_1, y_1) p^{K-1}(y_k)} \left[1 + \log \frac{e^{g(x_1, y_1)}}{m(x_1; y_{1:K})} \right] - \mathbb{E}_{p(x') p^K(y')} \left[\frac{e^{g(x'_1, y'_1)}}{m(x'_1; y'_{1:K})} \right] \end{aligned}$$

Due to the symmetry of $\{y_k\}_{k=1}^K$, we have

$$\mathbb{E}_{p(x') p^K(y')} \left[\frac{e^{g(x'_1, y'_1)}}{m(x'_1; y'_{1:K})} \right] = \mathbb{E}_{p(x') p^K(y')} \left[\frac{e^{g(x'_1, y'_k)}}{m(x'_1; y'_{1:K})} \right]. \quad (40)$$

So this gives

$$\mathbb{E}_{p(x') p^K(y')} \left[\frac{e^{g(x'_1, y'_1)}}{m(x'_1; y'_{1:K})} \right] = \mathbb{E}_{p(x') p^K(y')} \left[\frac{\frac{1}{K} e^{g(x'_1, y'_k)}}{m(x'_1; y'_{1:K})} \right] = 1, \quad (41)$$

which proves

$$I_{\text{NWJ}}(X_1, Y_{1:K}; \tilde{f}) = \mathbb{E}_{p(x_1, y_1) p^{K-1}(y_k)} \left[\log \frac{e^{g(x_1, y_1)}}{m(x_1; y_{1:K})} \right] \triangleq I_{\text{InfoNCE}} \quad (42)$$

Now we need to show this bound is sharp when $K \rightarrow \infty$. Recall the optimal $f(x, y)$ is given by $f^*(x, y) = \frac{p(y|x)}{p(y)}$.

$$\mathcal{L}_K^* = \mathbb{E}_{p^K} \left[\log \left(\frac{f^*(x_k, y_k)}{f^*(x_k, y_k) + \sum_{k' \neq k} f^*(x_k, y_{k'})} \right) \right] + \log K \quad (43)$$

$$= -\mathbb{E} \left[\log \left(1 + \frac{p(y)}{p(y|x)} \sum_{k'} \frac{p(y_{k'}|x_k)}{p(y_{k'})} \right) \right] + \log K \quad (44)$$

$$\approx -\mathbb{E} \left[\log \left(1 + \frac{p(y)}{p(y|x)} (K-1) \mathbb{E}_{y_{k'}} \frac{p(y_{k'}|x_k)}{p(y_{k'})} \right) \right] + \log K \quad (45)$$

$$= -\mathbb{E} \left[\log \left(1 + \frac{p(y_k)}{p(y_k|x_k)} (K-1) \right) \right] + \log K \quad (46)$$

$$\approx -\mathbb{E} \left[\log \frac{p(y)}{p(y|x)} \right] - \log(K-1) + \log K \quad (47)$$

$$(K \rightarrow \infty) \rightarrow I(X; Y) \quad (48)$$

This concludes our proof. \square

B Proof of Proposition 2.2 (FLO Properties)

Proof. Equation (17) is a direct consequence of applying the Fenchel duality trick to the UBA bound. We already know UBA is sharp when $g^*(x, y) = \log p(x|y) + c(x)$, and the Fenchel duality holds when $u^*(x, y; g) = \log \mathbb{E}_{p(y')} [\exp(g(x, y') - g(x, y))]$. So Equation (17) holds with $(g, u) = (g^*, u^*(g^*))$. We can also see this from equation (14). \square

C Proof of Corollary 2.3 (MI and $u(x, y)$)

Proof. This is immediate from equation (14). \square

D Gradient Analysis of FLO (More Detailed)

To further understand the workings of FLO, let us inspect the gradient of model parameters. Recall the intractable UBA MI estimator can be re-expressed in the following form:

$$I_{\text{UBA}'}(g_\theta) = \mathbb{E}_{p(x, y)} [-\log \mathbb{E}_{p(y')} [\exp(g_\theta(x, y') - g_\theta(x, y))]] \quad (49)$$

In this part, we want to establish the intuition that $\nabla_\theta \{I_{\text{FLO}}(u_\phi, g_\theta)\} \approx \nabla_\theta \{I_{\text{UBA}'}(g_\theta)\}$, where

$$I_{\text{FLO}}(u_\phi, g_\theta) \triangleq -\{u_\phi(x, y) + \mathbb{E}_{p(y')} [\exp(-u_\phi(x, y) + g_\theta(x, y') - g_\theta(x, y))]\} \quad (50)$$

is our FLO estimator.

By defining

$$\mathcal{E}_\theta(x, y) \triangleq \frac{1}{\mathbb{E}_{p(y')} [\exp(g_\theta(x, y') - g_\theta(x, y))]}, \quad (51)$$

we have

$$\nabla_\theta \left\{ \frac{1}{\mathcal{E}_\theta(x, y)} \right\} = -\frac{\nabla_\theta \mathcal{E}_\theta(x, y)}{(\mathcal{E}_\theta(x, y))^2} = -\frac{\nabla_\theta \log \mathcal{E}_\theta(x, y)}{\mathcal{E}_\theta(x, y)}, \quad (52)$$

and

$$\nabla_\theta \left\{ \frac{1}{\mathcal{E}_\theta(x, y)} \right\} = \nabla_\theta \mathbb{E}_{p(y')} [\{\exp(g_\theta(x, y') - g_\theta(x, y))\}] \quad (53)$$

$$= \mathbb{E}_{p(y')} [\nabla_\theta \{\exp(g_\theta(x, y') - g_\theta(x, y))\}]. \quad (54)$$

We know fixing $g_\theta(x, y)$, the corresponding optimal $u_\theta^*(x, y)$ maximizing FLO is given by

$$u_\theta^*(x, y) = \log \mathbb{E}_{p(y')} [\exp(g_\theta(x, y') - g_\theta(x, y))] = -\log \mathcal{E}_\theta(x, y). \quad (55)$$

This relation implies the view that $\exp^{-u_\phi(x,y)}$ is optimized to approximate $\mathcal{E}_\theta(x,y)$. And to emphasize this point, we now write $\hat{\mathcal{E}}_\theta(x,y) \triangleq e^{-u_\phi(x,y)}$. Assuming this approximation is sufficiently accurate (i.e., $\mathcal{E}_\theta \approx \hat{\mathcal{E}}_\theta$), we have

$$\nabla_\theta \{I_{\text{FLO}}(u_\phi, g_\theta)\} = -\mathbb{E}_{p(x,y)} \left[e^{-u_\phi(x,y)} \mathbb{E}_{p(y')} [\nabla_\theta \exp(g_\theta(x, y') - g_\theta(x, y))] \right] \quad (56)$$

$$= \mathbb{E}_{p(x,y)} \left[\frac{e^{-u_\phi(x,y)}}{\mathcal{E}_\theta(x,y)} \nabla_\theta \log \mathcal{E}_\theta(x,y) \right] \quad (57)$$

$$= \mathbb{E}_{p(x,y)} \left[\frac{\hat{\mathcal{E}}_\theta(x,y)}{\mathcal{E}_\theta(x,y)} \nabla_\theta \log \mathcal{E}_\theta(x,y) \right] \quad (58)$$

$$\approx \mathbb{E}_{p(x,y)} [\nabla_\theta \log \mathcal{E}_\theta(x,y)] \quad (59)$$

$$= \nabla_\theta \{ \mathbb{E}_{p(x,y)} [\log \mathcal{E}_\theta(x,y)] \} = \nabla_\theta \{I_{\text{UBA}'}(g_\theta)\}. \quad (60)$$

While the above relation shows we can use FLO to amortize the learning of UBA, one major caveat with the above formulation is that $\hat{u}(x,y)$ has to be very accurate for it to be valid. As such, one needs to solve a cumbersome nested optimization problem: update g_θ , then optimize u_ϕ until it converges before the next update of g_θ . Fortunately, we can show that is unnecessary: the convergence can be established under much weaker conditions, which justifies the use of simple simultaneous stochastic gradient descent for both (θ, ϕ) in the optimization of FLO.

E Proof of Proposition 2.4 (FLO Convergence)

Our proof is based on the convergence analyses of generalized stochastic gradient descent from [43]. We cite the main assumptions and results below for completeness.

Definition E.1 (Generalized SGD, Problem 2.1 [43]). Let $h(\theta; \omega), \omega \sim p(\omega)$ be an unbiased stochastic gradient estimator for objective $f(\theta)$, $\{\eta_t > 0\}$ is the fixed learning rate schedule, $\{\xi_t > 0\}$ is the random perturbations to the learning rate. We want to solve for $\nabla f(\theta) = 0$ with the iterative scheme $\theta_{t+1} = \theta_t + \tilde{\eta}_t h(\theta_t; \omega_t)$, where $\{\omega_t\}$ are iid draws and $\tilde{\eta}_t = \eta_t \xi_t$ is the randomized learning rate.

Assumption E.2. (Standard regularity conditions for Robbins-Monro stochastic approximation, Assumption D.1 [43]).

- A1. $h(\theta) \triangleq \mathbb{E}_\omega [h(\theta; \omega)]$ is Lipschitz continuous;
- A2. The ODE $\dot{\theta} = h(\theta)$ has a unique equilibrium point θ^* , which is globally asymptotically stable;
- A3. The sequence $\{\theta_t\}$ is bounded with prob 1;
- A4. The noise sequence $\{\omega_t\}$ is a martingale difference sequence;
- A5. For some finite constants A and B and some norm $\|\cdot\|$ on \mathbb{R}^d , $\mathbb{E}[\|\omega_t\|^2] \leq A + B\|\theta_t\|^2$ a.s. $\forall t \geq 1$.

Proposition E.3 (Generalized stochastic approximation, Proposition 2.2 [43]). Under the standard regularity conditions listed in Assumption E.2, we further assume $\sum_t \mathbb{E}[\tilde{\eta}_t] = \infty$ and $\sum_t \mathbb{E}[\tilde{\eta}_t^2] < \infty$. Then $\theta_n \rightarrow \theta^*$ with probability 1 from any initial point θ_0 .

Assumption E.4. (Weaker regularity conditions for generalized Robbins-Monro stochastic approximation, Assumption G.1 [43]).

- B1. The objective function $f(\theta)$ is second-order differentiable.
- B2. The objective function $f(\theta)$ has a Lipschitz-continuous gradient, i.e., there exists a constant L satisfying

$$-LI \preceq \nabla^2 f(\theta) \preceq LI,$$

- B3. The noise has a bounded variance, i.e., there exists a constant $\sigma > 0$ satisfying
- $$\mathbb{E} [\|h(\theta_t; \omega_t) - \nabla f(\theta_t)\|^2] \leq \sigma^2.$$

Proposition E.5 (Weaker convergence results, Proposition G.2 [43]). Under the technical conditions listed in Assumption E.4, the SGD solution $\{\theta_t\}_{t>0}$ updated with generalized Robbins-Monro

sequence $(\tilde{\eta}_t: \sum_t \mathbb{E}[\tilde{\eta}_t] = \infty \text{ and } \sum_t \mathbb{E}[\tilde{\eta}_t^2] < \infty)$ converges to a stationary point of $f(\theta)$ with probability 1 (equivalently, $\mathbb{E}[\|\nabla f(\theta_t)\|^2] \rightarrow 0$ as $t \rightarrow \infty$).

Proof. Since $\hat{\mathcal{E}}_{\theta_t}/\mathcal{E}_{\theta_t}$ is bounded between $[a, b]$ ($0 < a < b < \infty$), results follow by a direct application of Proposition E.3 and Proposition E.5. \square

F Gaussian Toy Model Experiments

First, we start validating the properties and utility of the proposed FLO estimator by comparing it to competing solutions with the Gaussian toy models, so that we also have the ground-truth MI for reference.

F.1 Choice of baselines

We choose TUBA, NWJ, InfoNCE and α -InfoNCE as our baselines. We set $\alpha = 0.8$ for the α -InfoNCE because among all other choices it better visualizes the bias-variance trade-offs relative to InfoNCE. NWJ and InfoNCE are the two most popular estimators in practice that are employed without additional hacks. TUBA is included for its close relevance to FLO (*i.e.*, optimizing $u(x)$ instead of $u(x, y)$, and being non-contrastive). We do not include DV here because we find DV needs excessively a large negative sample size K to work. Variants like MINE are excluded for involving additional tuning parameters or hacks which complicates analyses. The proposed FDV estimator is also excluded from our analyses for bound comparison since it includes \hat{I}_{DV} in the estimator. Note that although not suitable for MI estimation, we find FDV works quite well in representation learning settings where the optimization of MI is targeted. This is because in FDV, the primal term \hat{I}_{DV} term does not participate gradient computation, so it does not yield degenerated performance as that of DV.

F.2 Experimental setups

We use the following baseline setup for all models unless otherwise specified. For the critic functions $g(x, y)$, $u(x, y)$ and $u(x)$, we use multi-layer perceptron (MLP) network construction with hidden-layers 512×512 and ReLU activation. For optimizer, we use Adam and set learning rate to 10^{-4} . A default batch-size of 128 is used for training. To report the estimated MI, we use $10k$ samples and take the average. To visualize variance, we plot the decimal quantiles at $\{10\%, 20\%, \dots, 80\%, 90\%\}$ and color code with different shades. We sample fresh data point in each iteration to avoid overfitting the data. All models are trained for $\sim 5,000$ iterations (each epoch samples $10k$ new data points, that is 78 iterations per epoch for a total of 50 epochs).

For Figure 3, we use the 2-D Gaussian with $\rho = 0.5$, and the contour plot is obtained with a grid resolution of 2.5×10^{-2} .

For the shared parameterization experiment for FLO (Figure 5), we also used the more challenging 20-D Gaussian with $\rho = 0.5$, and trained the network with learning rate 10^{-3} and 10^{-4} respectively. We repeat the experiments for 10 times and plot the distribution of the MI estimation trajectories. The MLP network architecture we use was unable to get a sharp estimate in this setting (for other estimators too), but FLO with a shared network learns faster than its separate network counterpart, validating the superior efficiency of parameter sharing.

We setup the *bi-linear* critic experiment as follows. For the baseline FLO, we use the shared-network architecture for $g(x, y)$ and $u(x, y)$, and use the in-batch shuffling to create the desired number of negative samples (FLO-shuff). For FLO-BiL, we adopt the following implementation: feature encoders $h(x), \tilde{h}(y)$ are respectively modeled with three layer MLP with 512-unit hidden layers and ReLU activations, and we set the output dimension to 512. Then we concatenate the feature representation to $z = [h(x), \tilde{h}(y)]$ and fed it to the $u(x, y)$ network, which is a two-layer 128-unit MLP. Note that is merely a convenient modeling choice and can be further optimized for efficiency. Each epoch containing $10k$ samples, and FLO-shuff is trained with fixed batch-size. For FLO-BiL, it is trained with batch-size set to the negative sample-size desired, because all in-batch data are served as negatives. We use the same learning rate 10^{-4} for both cases, and this puts large-batch training at disadvantage, as fewer iterations are executed. To compensate for this, we use $T(K) = (\frac{K}{K_0})^{\frac{1}{2}} \cdot T_0$

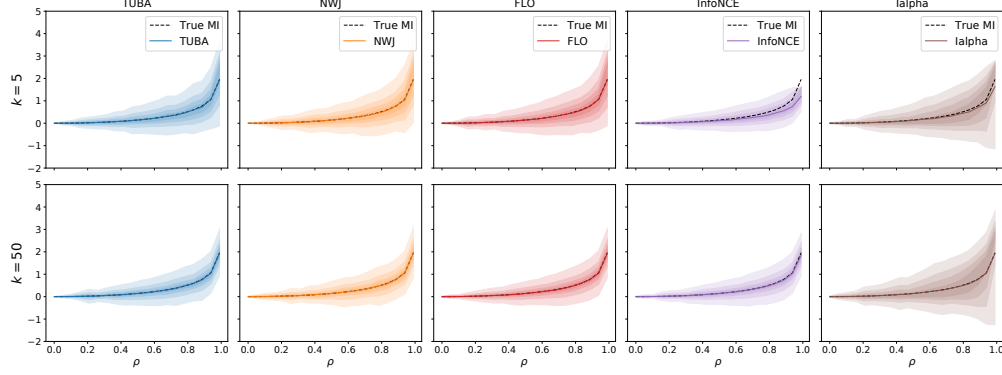


Figure S8: Bias variance plot for the popular MI bounds with the 2-D Gaussians. In this simpler case, TUBA, NWJ and FLO all give sharp estimate at $K = 5$. α -InfoNCE gives worst variance profile. The reason is that because α -InfoNCE interpolates between the low-variance multi-sample InfoNCE and high-variance single-sample NWJ (see Figure S10), and in this case the variance from NWJ dominates.

to set the total number of iterations for FLO-BiL, where (T_0, K_0) are respectively the baseline training iteration and negative sample size used by FLO-shuff, and the number of negative sample K are $\{10, 50, 100, 150, 200, 250, 300, 350, 400, 450, 500\}$. We are mostly interested in computation efficiency here so we do not compare the bound. In Figure 6, we see the cost for training FLO-shuff grows linearly as expected. For FLO-BiL, a U-shape cost curve is observed. This is because the network is roughly $2\times$ more complicated for the bi-linear implementation (*i.e.*, two more MLPs), and using a larger batch-size actually increases overall efficiency until the device capacity has been reached, which explains the initial drop in cost, followed by the anticipated square-root growth.

Cross-view representation learning experiment. In this experiment, we use the training split (*i.e.*, 60k) to train the cross-view representation and the prediction model based on the concatenated cross-view features. For CCA extraction, we use the `scikit-learn.cross_decomposition.CCA` implementation with default settings. For all other MI-based solutions, we use the multi-sample estimators and adopt the bi-linear critic implementation as described in the bi-linear experiment for maximal efficiency. The prediction model is given by a three-layer MLP of our standard configuration, and trained on the extracted cross-view features for 50 epochs with learning rate 10^{-3} .

F.3 Additional analyses and results

In Figure 4, all methods applied to 20D Gaussian (*i.e.*, that is 10 independent pairs of correlated x and y). We repeat in-batch shuffling K -times for the y -dimensions to get the desired number of negative samples.

Comprehensive analyses of bias-variance trade-offs. To supplement our results in the main paper, here we provide additional bias-variance plots for different MI estimators under various settings. In Figure S8 we show the bias-variance plot of MI estimates for 2-D Gaussians. In this case, the network used are sufficiently comprehensive so sharp estimate is attainable. In all cases the estimation variance grows with MI value, which is consistent with the theoretical prediction that for tight estimators, the estimation variance grows exponential with MI [33]. In such cases, the argument for InfoNCE’s low-variance profile no longer holds: it is actually performing sub-optimally. For complex real applications, the negative sample size used might not provide an adequate estimate of ground-truth MI (*i.e.*, the $\log K$ cap), and that is when InfoNCE’s low-variance profile actually helps. We also notice that, when the MI estimate is not exactly tight, but very close to the true value, the variance dropped considerably. This might provide alternative explanation (and opportunity) for the development near-optimal MI estimation theories, which is not covered in existing literature.

In Figure S9, we visualize the estimates for 20-D Gaussian with y randomly rotated and then passed through a cubic function. While in theory the MI should not be affected, as all the transformations applied are invertible; in practice, however, this is a more challenging problem for empirical estimation. The estimated MI bounds are looser compared to those with original y .

We also tried the single-sample estimators for NWJ, TUBA and FLO to their multi-sample InfoNCE-based counterparts (Figure S10), which is the comparison made by some of the prior studies. In

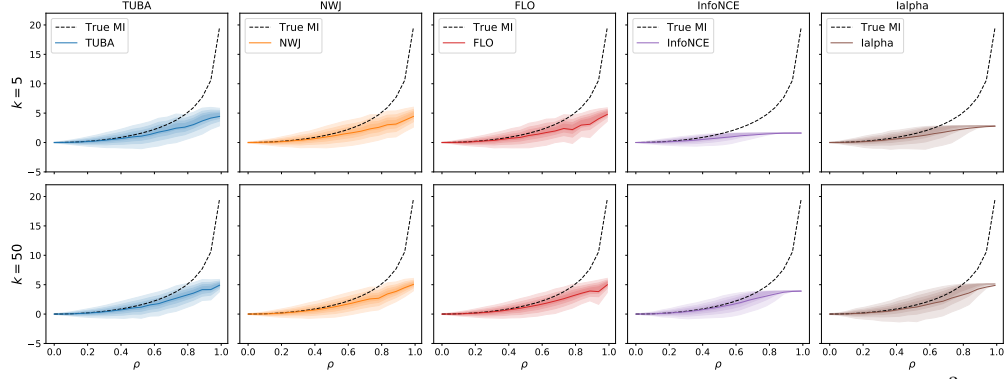


Figure S9: Bias variance plot for the popular MI bounds with the 10-D Gaussians with $(Ry)^3$, where R is a rotation matrix. Estimates are less tight compared with the original y .

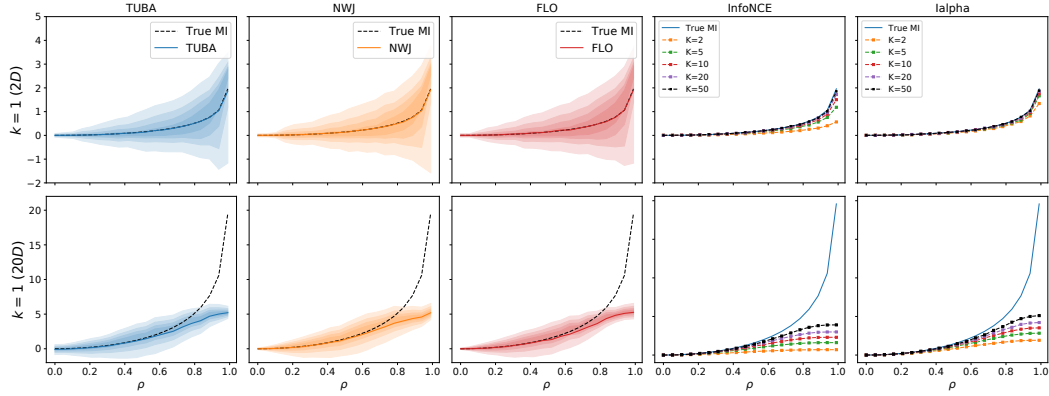


Figure S10: Bias variance plot for the popular MI bounds with the 2-D (upper panel) and 20-D (lower panel) Gaussians. Single-sample estimator of TUBA, NWJ and FLO (*i.e.*, $K = 1$) are compared to the multi-sample estimators of InfoNCE and α -InfoNCE.

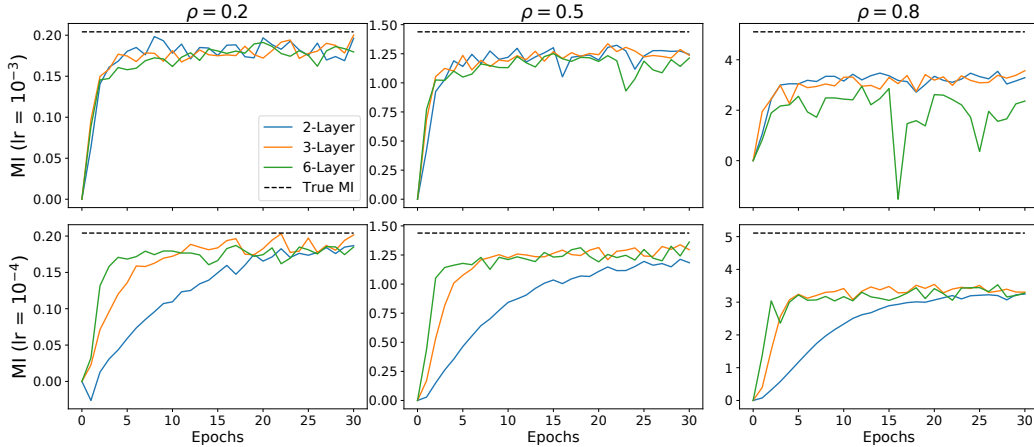


Figure S11: Ablation study for network complexity with FLO. More complex networks leads to faster convergence and better MI estimates. However, the stability is more sensitive to learning rate with a larger neural network.

this setting, the variance single-sample estimators' variances are considerably larger, which explains their less favorable performance. Note that contradictory to theoretical predictions, a larger negative sample size does make NWJ, TUBA and FLO tighter empirically, although the gains are much lesser compare to that of InfoNCE (partly because these three estimators are already fairly tight relative to InfoNCE). This might be explained by a better optimization landscape due to reduced estimation variance. We conjecture that for multi-sample NWJ, TUBA and FLO, the performance in empirical

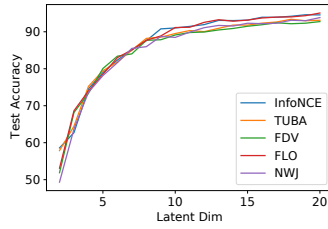


Figure S12: Extended results for the cross-view representation learning. FDV works best for smaller dimensions (≈ 5), and for higher dimensions (> 10) FLO and InfoNCE give the best results.

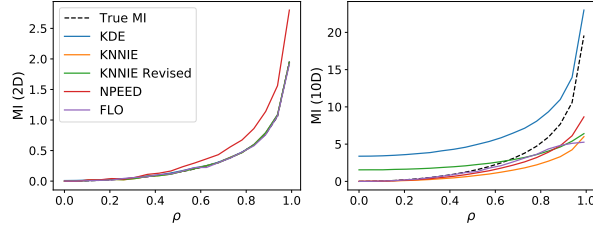


Figure S13: Extended results for the cross-view representation learning. We report the prediction accuracy for latent dimension from 2 to 20. FDV works best for smaller dimensions (≈ 5), and for higher dimensions (> 10) FLO and InfoNCE give the best results.

applications such as self-supervised learning should be competitive to that of InfoNCE, which has never been reported in literature.

Network capacity and MI estimation. We further investigate how the neural network learning capacity affect MI estimation. In Figure S11 we compare the training dynamics of the FLO estimator with L -layer neural networks, where $L \in \{2, 3, 6\}$ and each hidden-layer has 512-units. A deeper network is generally considered to be more expressive. We see that using larger networks in general converge faster in terms of training iterations, and also obtain better MI estimates. However, more complex networks imply more computation per iteration, and it can be less stable when trained with larger learning rates.

G Cross-view Representation Learning (Extended Analyses)

In addition to the results reported in the paper, we investigate how different latent dimension affect the results of the cross-view representation learning. We vary the latent dimension number from $d = 2$ to $d = 20$, and plot label prediction accuracy for the corresponding latent representations in Figure S12. The same setup for the bi-linear experiment is used for the MI estimation (for all MI estimators), where the images are flattened to be fed to the MLPs. The representations are trained for 50 epochs and the prediction model is trained for 50 epochs. We also trained the model for another 50 epochs and the conclusions are similar. We see that FDV works well for lower dimensions (*e.g.*, $d \approx 5$), and what works better for higher dimensions ($d > 10$) are FLO and InfoNCE.

H Comparison with Classical MI Estimators

We also compare our FLO estimator to the classical MI estimators. The following implementations of baseline estimators for multi-dimensional data are considered: (i) *KDE*: we use kernel density estimators to approximate the joint and marginal likelihoods, then compute MI by definition; (ii) *NPEET*⁷, a variant of Kraskov’s K -nearest neighbour (KNN) estimator [18, 56]; (iii) *KNNIE*⁸, the original KNN-estimator and its revised variant [57]. These models are tested on 2-D and 20-D Gaussians with varying strength of correlation, with their hyper-parameters tuned for best performance. Note that the notation of “best fit” is a little bit subjective, as we will fix the hyper-parameter for all dependency strength, and what works better for weak dependency might necessarily not work well for strong dependency. We choose the parameter whose result is visually most compelling. In addition to the above, we have also considered other estimators such as maximal-likelihood density ratio⁹ [24] and KNN with local non-uniformity correction¹⁰. However, these models either do not have a publicly available multi-dimensional implementation, or their codes do not produce reasonable results¹¹.

⁷<https://github.com/gregversteeg/NPEET>

⁸<https://github.com/wgao9/knnie>

⁹<https://github.com/leomuckley/maximum-likelihood-mutual-information>

¹⁰https://github.com/BiuBiuBiLL/NPEET_LNC

¹¹These are third-party python implementations, so BUGs are highly likely.

I Regression with Sensitive Attributes (Fair Learning) Experiments

I.1 Introduction to fair machine learning

Nowadays consequential decisions impacting people’s lives have been increasingly made by machine learning models. Such examples include loan approval, school admission, and advertising campaign, amongst others. While automated decision making has greatly simplified our lives, concerns have been raised on (inadvertently) echoing, even amplifying societal biases. Specially, algorithms are vulnerable in inheriting discrimination from the training data and passed on such prejudices in their predictions.

To address the growing need for mitigating algorithmic biases, research has been devoted in this direction under the name fair machine learning. While discrimination can take many definitions that are not necessarily compatible, in this study we focus on the most widely recognized criteria *Demographic Parity* (DP), as defined below

Definition I.1 (Demographic Parity, [52]). The absolute difference between the selection rates of a decision rule \hat{y} of two demographic groups defined by sensitive attribute s , *i.e.*,

$$\text{DP}(\hat{Y}, S) = \left| \mathbb{P}(\hat{Y} = 1 | S = 1) - \mathbb{P}(\hat{Y} = 1 | S = 0) \right|. \quad (61)$$

With multiple demographic groups, it is the maximal disparities between any two groups:

$$\text{DP}(\hat{Y}, S) = \max_{s \neq s'} \left| \mathbb{P}(\hat{Y} = 1 | S = s) - \mathbb{P}(\hat{Y} = 1 | S = s') \right|. \quad (62)$$

I.2 Experiment details and analyses

To scrub the sensitive information from data, we consider the *in-processing* setup

$$\mathcal{L} = \underbrace{\text{Loss}(\text{Predictor}(\text{Encoder}(x_i)), y_i)}_{\text{Primary loss}} + \lambda \underbrace{I(s_i, \text{Encoder}(x_i))}_{\text{Debiasing}}. \quad (63)$$

By regularizing model training with the violation of specified fairness metric $\Delta(\hat{y}, s)$, fairness is enforced during model training. In practice, people recognize that appealing to fairness sometimes cost the utility of an algorithm (*e.g.*, prediction accuracy) [58]. So most applications seek to find their own sweet points on the fairness-utility curve. In our example, it is the *DP-error* curve. A fair-learning algorithm is consider good if it has lower error at the same level of DP control.

In this experiment, we compare our MI-based fair learning solutions to the state-of-the-art methods. *Adversarial debiasing* tries to maximize the prediction accuracy for while minimize the prediction accuracy for sensitivity group ID [54]. We use the implementation from AIF360¹² package [59]. FERMI is a density-based estimator for the *exponential Rényi mutual information* $\text{ERMI} \triangleq \mathbb{E}_{p(x,y)} \left[\frac{p(x,y)}{p(x)p(y)} \right]$, and we use the official codebase. For evaluation, we consider the *adult* data set from UCI data repository [60], which is the 1994 census data with 30k samples in the train set and 15k samples in the test set. The target task is to predict whether the income exceeds \$50k, where gender is used as protected attribute. Note that we use this binary sensitive attribute data just to demonstrate our solution is competitive to existing solutions, where mostly developed for binary sensitive groups. Our solution can extend to more general settings where the sensitive attribute is continuous and high-dimensional.

We implement our fair regression model as follows. To embrace data uncertainty, we consider latent variable model $p_\theta(y, x, z) = p_\theta(y|z)p_\theta(x|z)p(z)$, where $v = \{x, y\}$ are the observed predictor and labels. Under the variational inference framework [61], we write the ELBO($v; p_\theta(v, z), q_\phi(z|v)$) as

$$\mathbb{E}_{Z \sim q_\phi(z|v)} [\log p_\theta(y|Z)] + \mathbb{E}_{Z \sim q_\phi(z|v)} [\log p_\theta(x|Z)] - \beta \text{KL}(q_\phi(z|v) \parallel p(z)) \quad (64)$$

$p(z)$ is modeled with standard Gaussian, and the approximate posterior $q_\phi(z|v)$ is modeled by a neural network parameterizing the mean and variance of the latents (we use the standard mean-field approximation so cross-covariance is set to zero), and β is a hyperparameter controlling the relative contribution of the KL term to the objective. Note that unlike in the standard ELBO we have dropped

¹²<https://github.com/Trusted-AI/AIF360>

Table S3: Self-supervised learning on MNIST with ResNet-50.

Model	NWJ	TUBA	InfoNCE	FLO	FDV
Accuracy	95.37	96.28	96.90	97.12	95.43

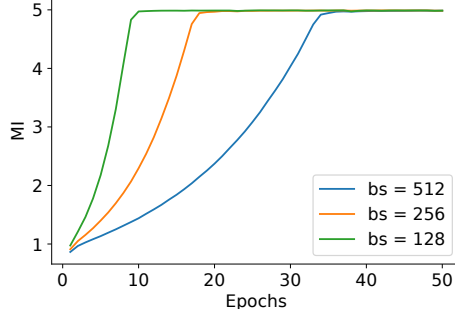


Figure S14: MI Estimation on Tiny-ImageNet

the term $\mathbb{E}_{Z \sim q_\phi(z|v)}[\log p_\theta(x|Z)]$ because we are not interested in modeling the covariates. Note this coincides with the *variational information bottleneck* (VIB) formulation [62]. Additionally, the posterior $q_\phi(z|v)$ will not be conditioned on y , but only on x , because in practice, the labels y are not available at inference time. All networks used here are standard three-layer MLP with 512 hidden-units.

For Figure 7, we note that the adversarial de-biasing actually crashed in the DP range $[0.1, 0.18]$, so the results have to be removed. Since interpolation is used to connect different data points, it makes the adversarial scheme look good in this DP range, which is not the case. FERMI also gave unstable estimation in the DP range $[0.1, 0.18]$. Among the MI-based solutions, NWJ was most unstable. Performance-wise, InfoNCE, TUBA and FDV are mostly tied, with the latter two slightly better in the “more fair” solutions (*i.e.*, at the low DP end).

J Self-supervised Learning

We further consider the self-supervised learning setup. In particular, we use MNIST data and a ResNet-10 network for feature extraction. To optimize representation without labels, we optimize the MI between two views of the digits: randomly rotated (0-30 degree) and resize & cropped (scale 0.5-1.0). We train with learning rate 10^{-4} for 50-epochs, and report the performance by training a linear classifier using the learned representation. See Table S3 for results. In this experiment, FLO worked best, followed by InfoNCE.

K Estimating MI on Tiny-ImageNet

In Figure S14 we show the MI estimation curve wrt training iterations on the tiny ImageNet dataset. We used a similar setup to the self-supervised learning experiment.